

# Decoding *active* force fluctuations from spatial trajectories of active systems

Anisha Majhi,<sup>1</sup> Biswajit Das,<sup>1</sup> Subhadeep Gupta,<sup>2,\*</sup> Anand Dev  
Ranjan,<sup>1</sup> Amirul Islam Mallick,<sup>2</sup> Shuvojit Paul,<sup>3,†</sup> and Ayan Banerjee<sup>1,‡</sup>

<sup>1</sup>Department of Physical Sciences, Indian Institute of Science Education and Research, Kolkata 741246, India

<sup>2</sup>Department of Biological Sciences, Indian Institute of Science Education and Research, Kolkata 741246, India

<sup>3</sup>Department of Physics, Kandi Raj College, Kandi, Murshidabad, West Bengal, 742137, India

(Dated: January 7, 2025)

Mesoscopic active systems exhibit various unique behaviours - absent in passive systems - due to the forces generated by the corresponding constituents by converting their available free energies. However, finding out these forces - which are also stochastic and remain intertwined with the thermal noise - is especially non-trivial. Here, we introduce a technique to extract such fluctuating active forces, with statistical accuracy, acting on a passive particle immersed in an active bath by filtering out the related thermal noise. First, we test the efficacy of our method under numerical scenarios and then apply it to the experimental trajectories of a microscopic particle (optically) trapped inside an active bath consisting of motile *E.Coli.* bacteria. We believe that our approach would be rather effective in the actual measurement of unknown active forces, which are a crucial component in processes involving living matter.

## I. INTRODUCTION:

Microscopic active systems, such as motile bacteria, active Brownian particles, etc., can produce their own forces and motion by exploiting their free energies (originating from internal physio-chemical processes) or utilizing proper external perturbations [1–3]. Due to these self-generated forces, these systems inherently stay away from equilibrium and can exhibit several complex collective phenomena [4, 5]. The behavior of embedded passive particles in fluids containing these active systems, i.e., *active fluids*, has also grown in interest enormously in recent times [6–12]. In such fluids, passive particles interact differently than in *passive fluids* and show several intriguing effects, including non-gaussian and enhanced diffusion [7, 9, 13, 14], occurrences of unidirectional motion of asymmetric passive particles [15, 16], and the emergence of long-range effective interactions between particles [17, 18]. The microscopic reason behind these behaviors is clearly the force acting on these passive particles from the active constituents in the fluid (this force can be called “*active force*”). The time-averaged nature of *active force* has been studied fairly elaborately, both theoretically and experimentally [19–23], and has displayed various interesting properties. For example, the average active force between passive particles shows wall curvature dependency [24, 25], Casimir-like effects [26], tunability depending on active constituent density [27], oscillating nature with distance [21] and constraint dependency [28]. However, only a few works exist to comprehend the fluctuation properties of the *active force*. Indeed, to explain the enhanced positional fluctuations

and multiple time scales (different from the diffusive time scaling  $\sim t$ ) present in the mean squared displacement function (MSD) of passive particles in *active fluids*, often the statistical nature of the underlying *active force* is considered as Gaussian distributed and exponentially correlated [10]. Nevertheless, such an assumption fails to explain the non-Gaussian properties repeatedly found in the positional fluctuations of passive particles immersed in active fluids [7–9]. It has been recently shown that an *active force* model with *poissonian active kicks* can be useful in this regard [29]. Clearly, the knowledge of the statistical nature of *active force* is extremely limited to date.

Further, without complete knowledge of *active force* fluctuations, the measurement of the thermodynamical parameters related to systems of passive particles in active fluids is rather insubstantial. It is known that, without the trajectory of force fluctuations, the irreversibility of the positional trajectories of passive particles measured using KL-divergence can be used as the only parameter to understand the thermodynamic effects of such systems [30]. However, KL-divergence generally provides an extreme lower bound of the total entropy production rate of the system. The availability of active force fluctuations could certainly provide the correct estimation of the total entropy production rate [31–33]. Moreover, thermodynamical quantities such as work and heat can also then be estimated using the usual trajectory energetics [34, 35].

Based on the above, it is apparent that a direct experimental measurement of *active force* trajectory should be really beneficial for developing soft matter physics related to active fluids from various aspects. However, to the best of our knowledge, no work is present to date that measures the whole fluctuating *active force* trajectory and the corresponding statistical properties directly acting on a passive particle in active fluids. Understandably, the reason behind this is that it is highly nontrivial as the thermally originated random force also remains

\* Present Address: London School of Hygiene and Tropical Medicine, Keppel Street, London WC1E 7HT, UK

† shuvojit.paul@krc.edu.in

‡ ayan@iiserkol.ac.in

added to the random *active force*, and one needs to correctly filter the thermal force out. Thus, here we propose a technique to infer the active force fluctuations from the positional fluctuations of a passive probe confined in an active environment. We demonstrate the efficacy of the model by both simulations and experiments, and observe that the model yields very good results - especially when the active force component is comparable or higher compared to the thermal force.

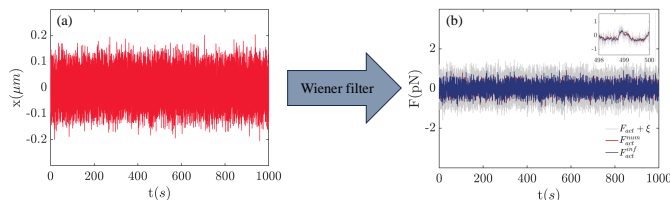


FIG. 1. Numerically generated position fluctuations of an optically trapped passive spherical particle are fed to the filter for obtaining filtered active force trajectory. (a) Positional trajectories of the particle. (b) Inferred active force ( $F_{act}^{inf}$ , in color blue) along with total force ( $F_{act}^{num} + \xi$ , in gray) and the active force used for the numerical simulation ( $F_{act}^{num}$ , in red) with time. Inset: expanded force trajectories to understand the efficacy of the method.

We choose a model system that is easily realizable in experiments to demonstrate our method; that is a harmonically trapped microscopic particle immersed in an active bath (see the Fig. 3(a)). The underlying dynamics of the particle localized inside the bath with an external harmonic potential of stiffness  $k$  can be described by the *Langevin* equation,

$$\gamma\dot{x}(t) + kx(t) = F(t) = \xi(t) + F_{act}(t), \quad (1)$$

where,  $x(t)$  denotes the one-dimensional position of the particle at time  $t$ , and  $\gamma$  ( $= 6\pi\eta a$ ) represents the related friction coefficient which depends on the radius of the microparticle ( $a$ ) and the viscosity of the medium ( $\eta$ ). The net force acting on the particle from the bath  $F(t)$  is the sum of the thermally originated delta correlated random force  $\xi(t)$ , i.e.  $\langle \xi(t) \rangle = 0$ ,  $\langle \xi(t)\xi(t') \rangle = 2k_B T \gamma \delta(t - t')$  and the stochastic force originating from the active constituents (e.g., motile bacteria, active Brownian particles, etc.) present only inside the bath, i.e.,  $F_{act}(t)$ . Here  $k_B$  denotes *Boltzmann* constant and  $T$  is the temperature of the bath. Due to the linearity of the *Langevin* equation,  $F(t)$  can be conveniently calculated from the position  $x(t)$  of the trapped particle if  $k$  and  $\gamma$  are known (see Eq. 1). Here, we show that  $\xi(t)$  from the net force  $F(t)$  can be filtered out to infer the active force  $F_{act}(t)$  exclusively. We first test our technique using numerical scenarios and then apply it to the experimentally recorded trajectories of a microscopic particle optically trapped inside motile bacteria baths of different concentrations.

The article is organized as follows: We first describe our technique in Section II, after which we evaluate its efficacy with a numerical scenario in Section III. Subsequently, in Section IV, we employ this technique to infer and comprehend active forces acting on a passive particle optically trapped inside an active bath comprised of motile *E. Coli.* cells. Lastly, we conclude our article with discussions and future directions in Section V.

## II. METHOD: BASED ON WIENER FILTER

Assuming the process to be stationary, we use the time domain Wiener filter to estimate the active part of the fluctuating time series of the force, i.e.,  $F_{act}(t)$  acting on the trapped probe particle [36]. Note that Brownian motion itself is a Wiener process [37], and the Wiener filter has been extensively used to remove random noise from a variety of data in image processing, signal processing, control systems, and digital communications, where the noise is additive [38]. In our case, as the properties of the thermally originated component of the force  $\xi(t)$  are known, with that also being uncorrelated to the active component  $F_{act}(t)$ , the Wiener filter can be efficiently employed. As described in the Eq. 1, the resultant force on the probe can be written as the following:

$$F(t) = F_{act}(t) + \xi(t), \quad (2)$$

and, for this system,  $F(t)$  is related to the trajectory of the probe  $x(t)$  as

$$F(t) = \gamma\dot{x}(t) + kx(t). \quad (3)$$

Note that the Wiener filter is a linear minimum mean-square-error estimator (LMMSE) that seeks a linear combination of  $\mathbf{F}$  so that the mean-square-error (MSE), i.e.,  $\langle (\mathbf{F}_{act} - \hat{\mathbf{F}}_{act})^2 \rangle$  becomes minimum. Here, the bold symbol represents a sequence, e.g.,  $\mathbf{F} = [F_i, i = 1, 2, 3, \dots, N]$ ,  $N$  is the total number of points. Now,  $\hat{\mathbf{F}}_{act}$  can be written as  $\hat{\mathbf{F}}_{act} = \mathbf{w}^T \mathbf{F}$ , and therefore the mean-square error,

$$\text{MSE} = \langle (\mathbf{F}_{act} - \mathbf{w}^T \mathbf{F})^2 \rangle. \quad (4)$$

Now to obtain the solution for  $\mathbf{w}$ , i.e.,  $\mathbf{w}^*$ , for which the MSE reaches the minimum, the gradient of the MSE with respect to  $\mathbf{w}$  should be zero. That is

$$\nabla_{\mathbf{w}} \text{MSE} = \nabla_{\mathbf{w}} \langle (\mathbf{F}_{act} - \mathbf{w}^T \mathbf{F})^2 \rangle = 0. \quad (5)$$

This finally leads to [36]

$$-\langle \mathbf{F}_{act} \mathbf{F} \rangle + \langle \mathbf{F} \mathbf{F}^T \rangle \mathbf{w} = 0. \quad (6)$$

Let  $\langle \mathbf{F}_{act} \mathbf{F} \rangle = \mathbf{r}$  be the *cross-correlation* vector between the resultant force and the active component, and  $\langle \mathbf{F} \mathbf{F}^T \rangle = \mathbf{R}$  is the *auto-correlation* matrix of  $\mathbf{F}$ . Therefore,

$$\mathbf{w}^* = \mathbf{R}^{-1} \mathbf{r}. \quad (7)$$

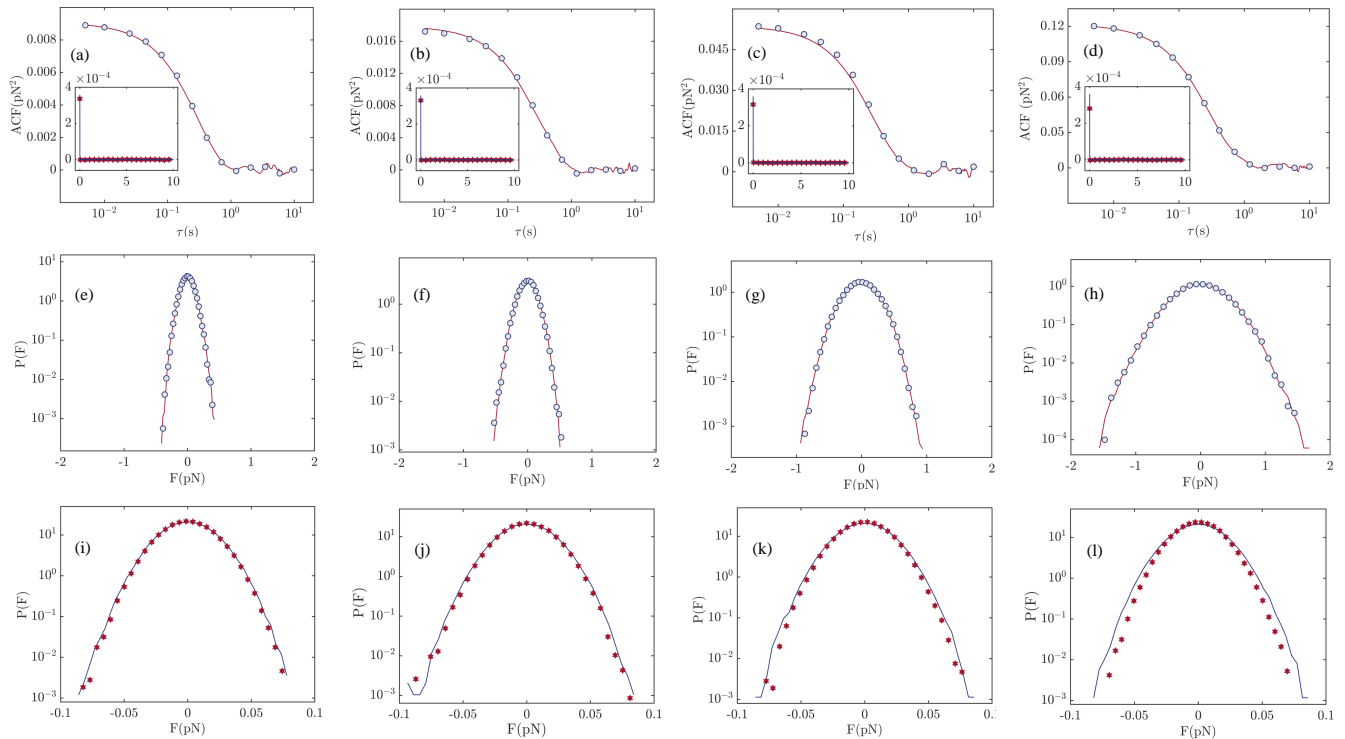


FIG. 2. **Top panel:** Autocorrelation function (ACF) plotted for numerically generated [*input*] active force (line) and inferred active force (circle) by filtering. Inset: ACF of the thermal force of numerical origin plotted against corresponding inferred (star) result. (a)-(d) are in the order of increasing activity strength, where  $d_f = 15, 30, 90, 200$  respectively. Corresponding normalised errors ( $\frac{\text{MSE}}{\text{Var}(F_{act})}$ ) are computed as,  $\sim 0.35, 0.26, 0.17, 0.11$  for  $d_f = 15, 30, 90, 200$  respectively. **Middle panel:** (e)-(h) shows the probability distribution function (PDF) of active forces (numerically generated (line) and numerically inferred (circle)) corresponding to increasing values of  $d_f$  as mentioned. **Bottom panel:** (i)-(l) PDF of the thermal force of numerical origin plotted with corresponding inferred (star) result in ascending order of activity strength. [Parameters that are fixed in the numerical simulation:  $k_B = 1.38 \times 10^{-23}$  J/K,  $T = 310$  K,  $a = 2.5$   $\mu\text{m}$ ,  $k = 7$  pN/ $\mu\text{m}$ ,  $\eta = 8.9 \times 10^{-4}$  Pa.s,  $\tau_e = 0.3$  s]

and

$$\hat{\mathbf{F}}_{act} = \mathbf{w}^* T \mathbf{F}. \quad (8)$$

Now, clearly from the Eq. 2, the *cross-correlation*  $\mathbf{r}$  is equal to the *auto-correlation* vector of  $\mathbf{F}_{act}$ , as  $\langle \mathbf{F}_{act} \xi \rangle = 0$ . Further, the *auto-correlation* vector of the active part of the force ( $\mathbf{F}_{act}$ ) can also be written as the difference between the *auto-correlation* vectors of  $\mathbf{F}$  and that of  $\xi$ . That is

$$\mathbf{r} = \langle \mathbf{F}_{act} \mathbf{F}_{act} \rangle = \langle \mathbf{F} \mathbf{F} \rangle - \langle \xi \xi \rangle. \quad (9)$$

Importantly, if the temperature of the system  $T$  is known, then obviously  $\langle \xi \xi \rangle$  is a vector with  $N - 1$  number of elements all having zero except the first element that is  $2k_B T \gamma$ , where  $k_B$  is the *Boltzmann* constant. Further, as  $\mathbf{F}$  can be calculated easily from the trajectory of the probe,  $\mathbf{R}$  and  $\mathbf{r}$  can also be determined. It is also because of this reason that it is advantageous to use the Wiener filter in this application, as by construction, it separates the forces based on statistical properties, unlike other non-adaptive methods (e.g. low-pass filters, moving average filters) which often fail to distinguish different stochastic forces in overlapping frequency ranges [39].

### III. NUMERICAL SCENARIO : ORNSTEIN UHLENBECK NOISE AS ACTIVE FORCE

First, we test our technique with numerical trajectories of a colloidal particle optically trapped in an active bath. The active force present in the bath is modelled as an exponentially correlated Ornstein-Uhlenbeck (OU) stochastic force with the correlation of the form:  $\langle F_{act}(t) F_{act}(t') \rangle = \gamma^2 D_e / \tau_e \exp(-(t - t') / \tau_e)$ , as it is often used for this purpose [10, 31]. To implement it numerically, the active force ( $F_{act}(t) \equiv \gamma \xi_{act}(t)$ ) can be represented by a stochastic variable ( $\xi_{act}(t)$ ) following a linear *Langevin* equation with drift  $-1/\tau_e$  and noise coefficient  $\sqrt{2D_e}/\tau_e$  [31, 33, 35]. The strength of the active force then can be denoted as  $D_e$ , which can be termed as the *active diffusion coefficient*. The correlation time of the force is denoted by  $\tau_e$ . We introduce a parameter  $d_f$  as the ratio of the active ( $D_e$ ) and thermal ( $D_0 = k_B T / \gamma$ ) diffusion coefficients, i.e.,  $d_f = D_e / D_0$ . Clearly, a higher value of  $d_f$  indicates a stronger contribution of the active force.

We vary the value of  $d_f$ , keeping all other parameters fixed, and generate trajectories of the trapped particle,

i.e.,  $x(t)$  for time 1000 secs with numerical time step 0.005 s. To generate these trajectories, the *Langevin* equations mentioned in Eq.(1) and that related to the active force are used to create a vector autoregressive model [40, 41] and then simulated using *varm* toolbox of MATLAB [42]. To match with experiments, we keep the trap stiffness fixed at  $k = 7$  pN/ $\mu\text{m}$  and  $\eta = 8.9 \times 10^{-4}$  Pa.s. The net force (active force plus the thermal force) on the particle is calculated following the Eq. 3. Further, the method described in the section II is followed to filter the thermal part from the net force, and to infer the active component only. Additionally, in the *Appendix B*, we have shown that a priori knowledge of the system time scale and thermal noise strength are not necessary for this method, which is an important highlight of this process. Indeed, both can be changed in the presence of many interacting particles in the bath. An initial presumption can be iteratively converged to the right values of these parameters with fairly high accuracy. One of the filtered trajectories is shown in Fig. 1(b), in which we describe our method pictorially. Note that the thermal force can be conveniently calculated by subtracting the inferred active force from the net force, and the corresponding statistical natures can also be calculated. The *auto-correlation function* (ACF) and the *probability density function* (PDF) of the estimated active force and the thermal force along with that of the known exact trajectories are shown in Fig. 2 for four values of  $d_f$ . The related errors of estimations are performed from the minimum of the MSE (Eq. 4), and their values normalized by the variance of the simulated active force are shown in Fig. 2. As expected, the accuracy of the filter monotonically increases with the increase of  $d_f$ . However, it is primarily limited by the finite length of the trajectory, which is further discussed in the *Appendix A*. Importantly, we find that the statistical parameters match considerably well for all the  $d_f$  values, as shown in Fig. 2. Note that the delta-correlation function and the Gaussian probability distribution function of the noise should be independent of  $d_f$ , and thus, they too should be utilized to check the correctness of the estimation (*see Appendix B*).

#### IV. EXPERIMENT: PASSIVE PARTICLE IN AN ACTIVE BACTERIAL BATH

We design an Optical Tweezers-based experimental arrangement to test the efficacy of our method and to infer the stochastic force from the experimental position fluctuations of a trapped microparticle. To create the optical trapping potential, we use the modular Optical Tweezers system (OTM, ThorLab) in which a Gaussian laser beam of wavelength 1064 nm is tightly focused by an objective lens of high numerical aperture ( $\text{NA} = 1.4$ , 100X, oil-immersion) installed in a conventional inverted microscope (NIKON). Silica microparticles (diameter 5  $\mu\text{m}$ ) - sparsely dispersed in a bath of motile *E.coli* cells - are

trapped inside a sample holder placed on a temperature-controlled stage. The sample holder is prepared by attaching a Polyethylene glycol (PEG) coated glass coverslip at the bottom of an aluminium plate with a circular hole. The top surface is then sealed by attaching another coverslip, creating a circular cavity of diameter 14 mm and height 1 mm. All edges and contact points between the aluminum plate and glass coverslips are ensured to be perfectly sealed to eliminate air contact. PEG coating prevents sticking and accumulation of *E.coli* cells at the bottom of coverslips, which would hamper the uniformity of the bacterial concentration over time. The details of preparing the particle-cell mixture are given in *Appendix C*. Note that the size of the enclosed sample chamber is much larger than *E.coli* cells ( $\sim 3$   $\mu\text{m}$ ) and the trapped probe particle, so that it can be considered isotropic and homogeneous over the length scale of the system - which further eliminates the possibility of observing persistent rotation of the probe particle inside the bacterial bath. To detect the position fluctuations of the trapped particle, images of the particle are captured at 200 Hz using a camera (ThorLabs) attached to the microscope for approximately 300 s. The centre of the particle in each frame is then located using a standard particle tracking algorithm provided in Ref. [43].

We record the position fluctuations of the trapped particle in three separate concentrations of the bacterial solution (Conc 1:  $2 \times 10^5$  CFU, Conc 2:  $1 \times 10^6$  CFU, Conc 3:  $5 \times 10^6$  CFU, where ‘CFU’ stands for ‘Colony Forming Units’), kept at temperature  $T = 37^\circ\text{C}$ . The stiffness constant of the trap remains fixed at  $k = 7.0 \pm 0.5$  pN/ $\mu\text{m}$  throughout the experiments. We observe that the fluctuations of the probe particle in the bacterial bath with concentration  $\sim 10^5$  CFU remain Gaussian (Fig. 3(b)) and the corresponding active force fluctuations inferred from the trajectory also maintain Gaussian characteristics (Fig. 3(f)). However, the probability distributions (PDF) of the position fluctuations of the probe particle are found to be non-Gaussian for the active baths with higher bacterial concentration as shown in Figs. 3(c) and 3(d). The variance of the Gaussian core is also enhanced with the concentration of the bacteria. Note that non-Gaussian PDFs with prominent tails at the edges indicate that the effective active force on the probe particle from the bacterial baths with concentrations  $\geq 10^6$  CFU (within our experimental scenarios) may not be Gaussian but rather possess some non-Gaussian characteristics - which are beyond the scope of usual Ornstein-Uhlenbeck (OU) modelling of active forces [10]. Indeed, our analysis reveals that non-Gaussian features are clearly present in the corresponding active forces computed from the experimental trajectories (Figs. 3(g) and 3(h)).

To account for the appearance of the exponential tails along with the broadening of the Gaussian core, the probability distribution functions of both positional fluctuations ( $x(t)$ ) and active force fluctuations ( $F(t)$ ) are fitted (Fig. 3(e) and Fig. 3(i)) with a weighted sum of Gaussian and exponential distributions as [7]:  $P(y) =$

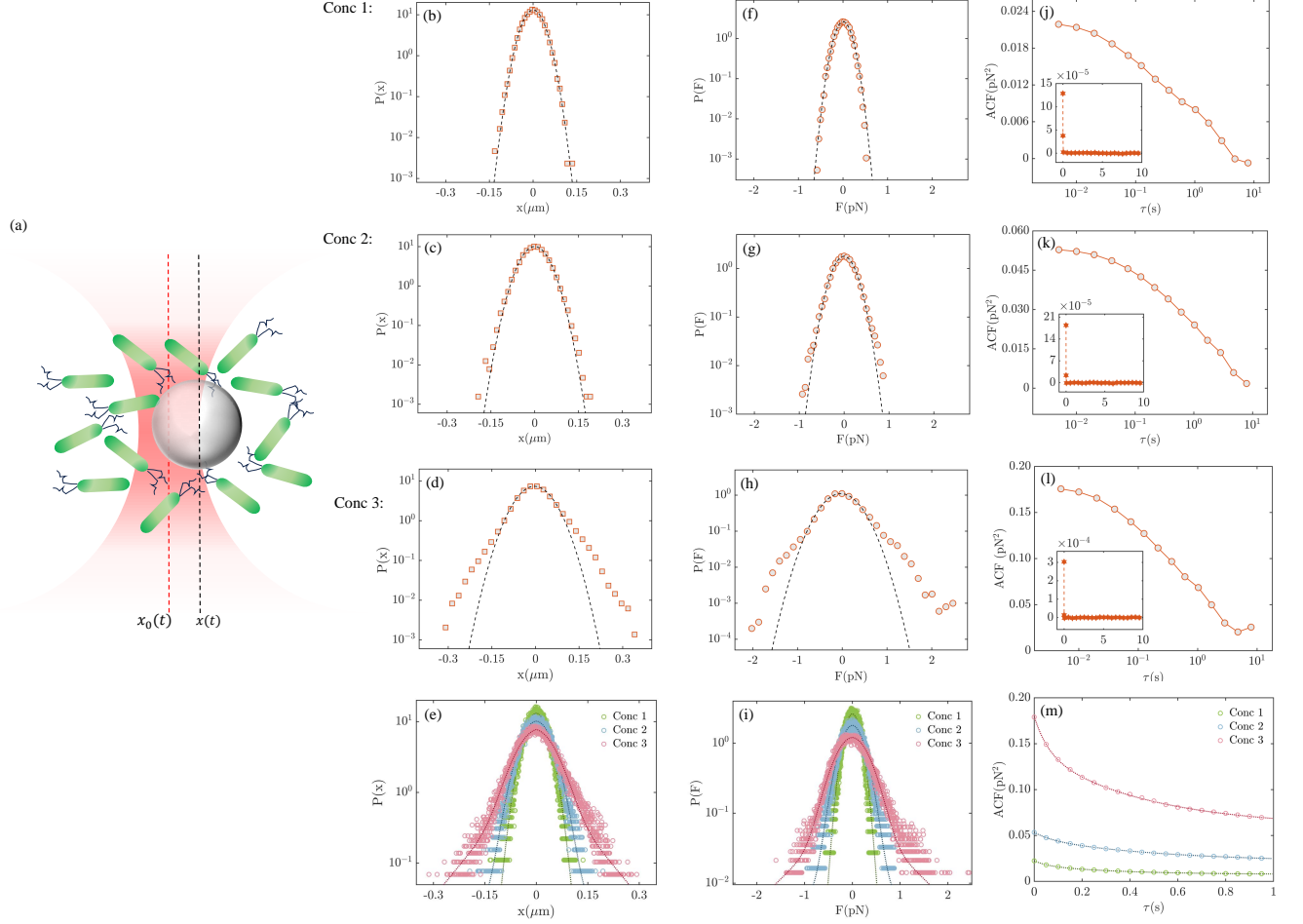


FIG. 3. (a) Schematic of an optically confined passive probe in motile *E.coli* bath. Experiments are performed for three different concentrations of active cells. Conc 1:  $2 \times 10^5$  CFU, conc 2:  $1 \times 10^6$  CFU, conc 3:  $5 \times 10^6$  CFU where CFU stands for colony forming units). (b)-(d) The probability distribution functions ( $P(x)$ ) corresponding to the experimentally recorded position fluctuations of the passive probe in the active *e.coli* bath with different concentrations are shown. The dotted lines indicate the Gaussian core of  $P(x)$ . (e) The deviation from Gaussian characteristics of  $P(x)$  at higher bacterial concentrations is indicated through the empirical fits. Corresponding function is described as  $P(y)$  in the main text. (f)-(h) The probability distribution functions of the inferred active forces ( $P(F)$ ) from the experimental trajectories for different bacterial concentrations are plotted. (i)  $P(F)$  corresponding to all the concentrations are empirically fitted with non-Gaussian functions, described as  $P(y)$  in the main text. (j)-(l) Autocorrelation function (ACF) of the inferred active forces are shown and ACFs of the thermal forces extracted from corresponding trajectories are shown in insets. (m) ACFs of the inferred active forces are fitted with double-exponential functions with different decay rates.

$\frac{1-f}{\sqrt{2\pi}\sigma_g^2} \exp(-\frac{y^2}{2\sigma_g^2}) + \frac{f}{2\sigma_e} \exp(-\frac{|y|}{\sigma_e})$ . Here, the parameter  $\sigma_g$  denotes the standard deviation of the Gaussian distribution,  $\sigma_e$  is the decay length of the exponential distribution and  $f(0 \leq f < 1)$  indicates the fractional contribution of the enhanced displacement or force.

Moreover, the computed active forces of the bacterial baths are correlated as depicted in Figs. 3(j) - 3(l). To explore it further, we fit the time-dependent autocorrelation functions (ACF) of the corresponding active forces with a double exponential function:  $f(t) = A_1 \exp(-t/\tau_1) + A_2 \exp(-t/\tau_2)$ , as has also been done in Ref. [1]. We assume that the short-time autocorrelation function is a monotonically decaying function with

at least two relaxation timescales ( $\tau_1$  and  $\tau_2$ ), and the corresponding coefficients ( $A_1$  and  $A_2$ ) should be related to the (diffusion) strength of the active forces [22].

From the empirical fit shown in Fig. 3(m), we find that both  $\tau_1$  and  $\tau_2$  almost remain constant with the bacterial concentrations in the bath and  $\tau_1 \ll \tau_2$ . Quantitatively, we estimate the longer timescale to be  $\tau_2 = (0.46 \pm 0.11)$  s over the concentrations - which is comparable to the typical persistent timescales of the motile *E.Coli* cells [10], and the value of  $\tau_1$  is at least one order less than  $\tau_2$  - which may appear due to the (steric) interaction between the passive probe and the motile bacteria. Furthermore, it is expected that the coefficient related to

	$A_1(\times 10^{-3}\text{pN}^2)$	$\tau_1(\text{s})$	$A_2(\times 10^{-3}\text{pN}^2)$	$\tau_2(\text{s})$
Conc 1	$4.342 \pm 0.236$	$0.052 \pm 0.004$	$10.05 \pm 0.1920$	$0.344 \pm 0.013$
Conc 2	$7.019 \pm 0.499$	$0.079 \pm 0.007$	$25.093 \pm 0.231$	$0.561 \pm 0.029$
Conc 3	$35.274 \pm 1.210$	$0.059 \pm 0.003$	$81.363 \pm 0.722$	$0.463 \pm 0.016$

TABLE I. Time dependent autocorrelation functions (ACF) of inferred active forces are fitted by a double exponential function of the form,  $f(t) = A_1 \exp(-t/\tau_1) + A_2 \exp(-t/\tau_2)$ . The respective values of the corresponding fitting parameters along with errors are tabulated here.

the slow timescale ( $\tau_2$ ) i.e.  $A_2$  should carry the signature of the strength of active diffusion in different concentrations of bacteria. Taking into account  $A_2 \equiv \gamma^2 D_e / \tau_2$ , we estimate the active diffusion constants for the three concentrations as,  $D_e[\text{Conc 1}] = 1.97 \mu\text{m}^2/\text{s}$ ,  $D_e[\text{Conc 2}] = 8 \mu\text{m}^2/\text{s}$  and  $D_e[\text{Conc 3}] = 21.42 \mu\text{m}^2/\text{s}$ . The estimated active diffusion constants are evidently higher

than the thermal diffusion ( $k_B T / \gamma \sim 0.1 \mu\text{m}^2/\text{s}$ ). The other coefficient  $A_1$  is found to be significantly lower than  $A_2$  and the effect of this coefficient in estimating the strength of active diffusion can be neglected as  $A_1 \tau_1 \ll A_2 \tau_2$ . The details of the fitting parameters and the subsequent estimations of the active diffusion constants are tabulated in TABLE I.

## V. CONCLUSIONS:

In summary, we have numerically and experimentally demonstrated that the fluctuating active force on a spatially confined passive particle in an active fluid can be measured with high statistical accuracy by isolating the intertwined thermally induced random force. In doing so, this study has also revealed the true statistical characteristics of the active force, which is non-Gaussian and exhibits multi-exponential correlations. When the probability distribution function of the active force is modeled as a weighted sum of Gaussian and exponential distributions, the corresponding auto-correlation function fits a double-exponential form, with the larger time scale comparable to that of the active components. Additionally, a smaller time scale may arise from steric interactions among the constituents. It is important to note that our demonstrated method of inferring active force trajectory is independent of the nature of the force. Moreover, it requires minimal information about the system and is based on explicitly measurable quantities. Finally, this approach can be extended to systems involving multiple passive particles, enabling the measurement of thermodynamic properties [31] with significantly enhanced precision. A very useful extension would also be for viscoelastic fluids, where the presence of memory would definitely lead to complications, but a solution would be very useful for living matter systems which are inherently viscoelastic, and where activity is widely present. We are working in these areas, and hope to report interesting results in the future.

## Appendix A: Filter accuracy: Dependence on the sampling time interval and total sampling time

The mean square error (MSE), as described in the main text (see *section III*), is observed as a function of varying input parameters, such as sampling time step or rate ( $\delta t$ ) and total sampling time ( $T_s$ ). In Fig. 4(a), with a fixed sampling time ( $T_s = 1000$  s), MSE increases by around 4 % with the increase of  $\delta t$  over one order of magnitude. Understandably, when  $\delta t$  is well below the characteristic timescale ( $\approx 0.006$  s for this case) of the system, the accuracy converges towards the maximum, and the MSE tends to the minimum.

Further, with the total sampling time and for a fixed  $\delta t (= 0.005$  s), in Fig. 4(b), reasonably, MSE declines for ascending values of ' $T_s$ '. However, the improvement in accuracy for this case is around 6 % for an increase of  $t$  from 300 to 5000 s. Further increase in  $t$  does not seem to increase the accuracy any significantly.

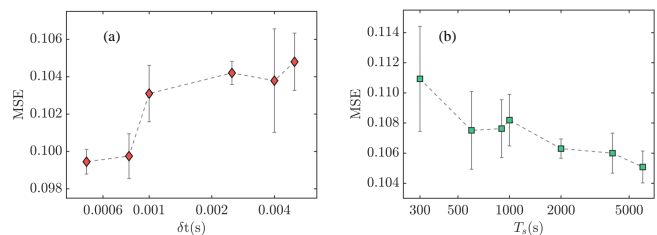


FIG. 4. Mean square error (MSE) plotted for various sampling rate ( $\delta t$ ) and total time ( $T_s$ ). Error bars represent standard deviations averaged over multiple independent inputs of  $\delta t$  and  $t$ .

## Appendix B: Optimization based on the system time scale and the thermal noise strength:

Theoretically, one would expect that the trapped particle inside the active bacterial bath will follow the *Langevin* equation - which can be discretized for the filtering purpose - as:  $x_{t+dt} = x_t - (k/\gamma)x_t dt + (F_t^{act}/\gamma)dt + \sqrt{2k_B T dt/\gamma} \eta_t$  with  $\eta_t \sim \mathcal{N}(0, 1)$ . However, due to the presence of the bacteria in the bath, the time scale of the system, i.e.,  $\gamma/k$  can be modified, and it should also be reflected in the strength of the thermal noise. Nonetheless, the statistical nature of the noise should remain unchanged with the subtle variations in the noise strength. Therefore, we write the variance of the noise as  $\alpha k_B T/\gamma$  (where theoretically  $\alpha$  should be equal to 2), and iteratively vary the inverse timescale  $k/\gamma$  and  $\alpha$  to obtain the noise with properties the same as known previously. For example, in Fig. 5, we show how the autocorrelation function of random forces ( $\xi_{theory} \sim \mathcal{N}(0, 2k_B T\gamma)$ ) varies with these two parameters with respect to the reference known properties. Clearly, for typical experimental data, the deviation of the ACF from the theoretically expected nature is the minimum for certain values of  $\alpha$  and  $k/\gamma$  (for the highest concentration, i.e., Conc 3, these are  $\alpha \approx 2.1$  and  $k/\gamma \approx 190 \text{ s}^{-1}$ ) as shown in Fig. 5(a)-(b). We also show this for numerically simulated trajectories in Fig. 5(c)-(d). Note that the ACFs of the inferred random forces from the numerical trajectories are with the least error for  $\alpha \approx 2$  and  $k/\gamma \approx 167 \text{ s}^{-1}$  as these are the actual values of the parameters used to generate the trajectories. The corresponding *Errors* for each parameter sweep are plotted as the insets of Fig. 5(a)-(d), and it is defined as,  $Error = |ACF(Inferred \text{ random force}) - ACF(theory)|/(2k_B T\gamma)$ .

## Appendix C: Sample preparation: Ecoli culture

*Motile E.Coli* (DH5a) cells are used as active particles. To facilitate differential count and imaging, *E. coli* cells were transformed with the pTurboGFP-B plasmid (kindly provided by Dr. P. P. Dutta, IISER Kolkata) by the heat shock method [44]. Positive transformants were selected on the basis of antibiotic selection, green fluorescence, and colony PCR. Next, GFP expressing-*E.coli* were grown in Luria-Bertani (LB) medium (HiMedia, India) at 37°C, supplemented with ampicillin (100 µg/mL).

The density of the bacterial culture was adjusted to an optical density (OD) of 0.7 at 600 nm, corresponding to approximately  $1 \times 10^7$  CFU/mL, as determined using a spectrophotometer. A 1 mL aliquot of the bacterial culture was pelleted by centrifugation at 4000 rpm for 7 minutes. The resulting pellet was resuspended in 1 mL of distilled water. The bacterial concentration was further adjusted according to the desired density.

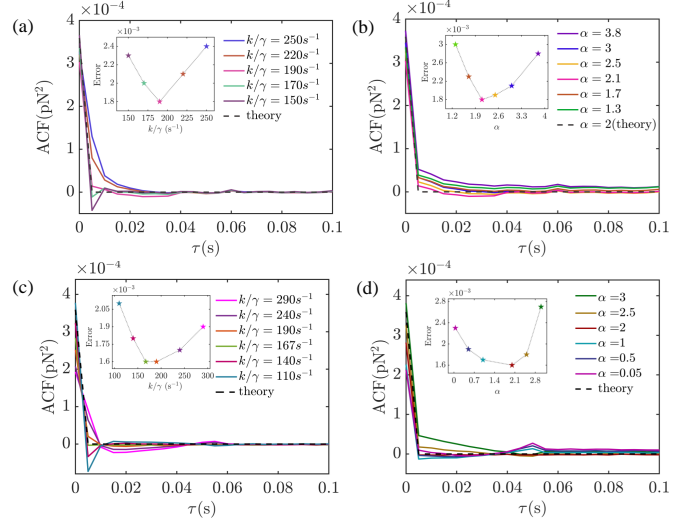


FIG. 5. (a)-(b) Experimental (for the highest active strength; i.e., Conc 3): The variation of ACF of thermal forces from its anticipated theoretical value minimizes for a particular measure of  $\alpha$  and  $k/\gamma$ . In (a)  $\alpha$  is fixed at 2.1 and in (b)  $k/\gamma$  is fixed at  $190 \text{ s}^{-1}$ . (c)-(d) Numerical: The deviation of ACFs of the inferred thermal forces are observed by varying the parameters  $\alpha$  and  $k/\gamma$  (for highest active strength, i.e.,  $d_f = 200$ ). In (c)  $\alpha = 2$  and in (d)  $k/\gamma = 167 \text{ s}^{-1}$  are fixed. The corresponding errors for (a)-(d) are shown in the insets.

## ACKNOWLEDGMENTS

The work is supported by IISER Kolkata, and the Science and Engineering Research Board (SERB), Department of Science and Technology, Government of India, through the research grant CRG/2022/002417. SP is thankful to Kandi Raj College for its support. BD is thankful to the Ministry Of Education of Government of India for financial support through the Prime Minister's Research Fellowship (PMRF) grant.

[1] E. Fodor, C. Nardini, M. E. Cates, J. Tailleur, P. Visco, and F. van Wijland, How far from equilibrium is active matter?, *Physical Review Letters* **117**, 038103 (2016).  
 [2] S. Ramaswamy, Active matter, *Journal of Statistical Mechanics: Theory and Experiment* **2017**, 054002 (2017).  
 [3] M. t. Vrugt and R. Wittkowski, A review of active matter reviews, *arXiv preprint arXiv:2405.15751* (2024).

[4] C. Bechinger, R. Di Leonardo, H. Löwen, C. Reichhardt, G. Volpe, and G. Volpe, Active particles in complex and crowded environments, *Reviews of Modern Physics* **88**, 045006 (2016).  
 [5] M. J. Bowick, N. Fakhri, M. C. Marchetti, and S. Ramaswamy, Symmetry, thermodynamics, and topology in active matter, *Physical Review X* **12**, 010501 (2022).

- [6] X.-L. Wu and A. Libchaber, Particle diffusion in a quasi-two-dimensional bacterial bath, *Physical Review Letters* **84**, 3017 (2000).
- [7] K. C. Leptos, J. S. Guasto, J. P. Gollub, A. I. Pesci, and R. E. Goldstein, Dynamics of enhanced tracer diffusion in suspensions of swimming eukaryotic microorganisms, *Physical Review Letters* **103**, 198103 (2009).
- [8] A. Argun, A.-R. Moradi, E. Pinçe, G. B. Bağcı, A. Imparato, and G. Volpe, Non-boltzmann stationary distributions and nonequilibrium relations in active baths, *Physical Review E* **94**, 062150 (2016).
- [9] L. Ortlieb, S. Rafai, P. Peyla, C. Wagner, and T. John, Statistics of colloidal suspensions stirred by microswimmers, *Physical Review Letters* **122**, 148101 (2019).
- [10] C. Maggi, M. Paoluzzi, N. Pellicciotta, A. Lepore, L. Angelani, and R. Di Leonardo, Generalized energy equipartition in harmonic oscillators driven by active baths, *Physical Review Letters* **113**, 238303 (2014).
- [11] Y. B. Dor, Y. Kafri, M. Kardar, and J. Tailleur, Passive objects in confined active fluids: A localization transition, *Phys. Rev. E* **106**, 044604 (2022).
- [12] J. Reichert and T. Voigtmann, Tracer dynamics in crowded active-particle suspensions, *Soft Matter* **17**, 10492 (2021).
- [13] A. Lagarde, N. Dagès, T. Nemoto, V. Démery, D. Bartolo, and T. Gibaud, Colloidal transport in bacteria suspensions: from bacteria collision to anomalous and enhanced diffusion, *Soft Matter* **16**, 7503 (2020).
- [14] H. Nordanger, A. Morozov, and J. Stenhammar, Anisotropic diffusion of ellipsoidal tracers in microswimmer suspensions, *Phys. Rev. Fluids* **7**, 013103 (2022).
- [15] R. Di Leonardo, L. Angelani, D. Dell'Arciprete, G. Ruocco, V. Iebba, S. Schippa, M. P. Conte, F. Mecarini, F. De Angelis, and E. Di Fabrizio, Bacterial ratchet motors, *Proceedings of the National Academy of Sciences* **107**, 9541 (2010).
- [16] A. Sokolov, M. M. Apodaca, B. A. Grzybowski, and I. S. Aranson, Swimming bacteria power microscopic gears, *Proceedings of the National Academy of Sciences* **107**, 969 (2010).
- [17] M. Zaeifi Yamchi and A. Naji, Effective interactions between inclusions in an active bath, *The Journal of chemical physics* **147** (2017).
- [18] Y. Baek, A. P. Solon, X. Xu, N. Nikola, and Y. Kafri, Generic long-range interactions between passive bodies in an active fluid, *Phys. Rev. Lett.* **120**, 058002 (2018).
- [19] J. P. Hernandez-Ortiz, C. G. Stoltz, and M. D. Graham, Transport and collective dynamics in suspensions of confined swimming particles, *Phys. Rev. Lett.* **95**, 204501 (2005).
- [20] L. Angelani, C. Maggi, M. L. Bernardini, A. Rizzo, and R. Di Leonardo, Effective interactions between colloidal particles suspended in a bath of swimming cells, *Phys. Rev. Lett.* **107**, 138302 (2011).
- [21] S. Paul, A. Jayaram, N. Narinder, T. Speck, and C. Bechinger, Force generation in confined active fluids: The role of microstructure, *Physical Review Letters* **129**, 058001 (2022).
- [22] A. Jayaram and T. Speck, Effective dynamics and fluctuations of a trapped probe moving in a fluid of active hard discs (a), *Europhysics Letters* **143**, 17005 (2023).
- [23] J. Shea, G. Jung, and F. Schmid, Force renormalization for probes immersed in an active bath, *Soft Matter* **20**, 1767 (2024).
- [24] A. P. Solon, Y. Fily, A. Baskaran, M. E. Cates, Y. Kafri, M. Kardar, and J. Tailleur, Pressure is not a state function for generic active fluids, *Nature physics* **11**, 673 (2015).
- [25] F. Smallenburg and H. Löwen, Swim pressure on walls with curves and corners, *Phys. Rev. E* **92**, 032304 (2015).
- [26] D. Ray, C. Reichhardt, and C. J. O. Reichhardt, Casimir effect in active matter systems, *Phys. Rev. E* **90**, 013019 (2014).
- [27] R. Ni, M. A. Cohen Stuart, and P. G. Bolhuis, Tunable long range forces mediated by self-propelled colloidal hard spheres, *Phys. Rev. Lett.* **114**, 018302 (2015).
- [28] P. Liu, S. Ye, F. Ye, K. Chen, and M. Yang, Constraint dependence of active depletion forces on passive particles, *Phys. Rev. Lett.* **124**, 158001 (2020).
- [29] C. Di Bello, R. Majumdar, R. Marathe, R. Metzler, and É. Roldán, Brownian particle in a poisson-shot-noise active bath: Exact statistics, effective temperature, and inference, *Annalen der Physik* , 2300427 (2024).
- [30] É. Roldán, J. Barral, P. Martin, J. M. Parrondo, and F. Jülicher, Quantifying entropy production in active fluctuations of the hair-cell bundle from time irreversibility and uncertainty relations, *New Journal of Physics* **23**, 083013 (2021).
- [31] L. Dabelow, S. Bo, and R. Eichhorn, Irreversibility in active matter systems: Fluctuation theorem and mutual information, *Physical Review X* **9**, 021009 (2019).
- [32] S. K. Manikandan, S. Ghosh, A. Kundu, B. Das, V. Agrawal, D. Mitra, A. Banerjee, and S. Krishnamurthy, Quantitative analysis of non-equilibrium systems from short-time experimental data, *Communications Physics* **4**, 258 (2021).
- [33] B. Das, S. K. Manikandan, S. Paul, A. Kundu, S. Krishnamurthy, and A. Banerjee, Tuning irreversibility of mesoscopic processes using hydrodynamic interactions, *arXiv preprint arXiv:2405.00800* (2024).
- [34] K. Sekimoto, Langevin equation and thermodynamics, *Progress of Theoretical Physics Supplement* **130**, 17 (1998).
- [35] B. Das, S. Paul, S. K. Manikandan, and A. Banerjee, Enhanced directionality of active processes in a viscoelastic bath, *New Journal of Physics* **25**, 093051 (2023).
- [36] N. Wiener, *Extrapolation, interpolation, and smoothing of stationary time series: with engineering applications* (The MIT press, 1949).
- [37] N. Wiener, Differential-space, *Journal of Mathematics and Physics* **2**, 131 (1923).
- [38] D. Boulfefel, R. Rangayyan, L. Hahn, and R. Kloiber, Three-dimensional restoration of single photon emission computed tomography images, *IEEE transactions on nuclear science* **41**, 1746 (1994).
- [39] P. S. Diniz, *Adaptive filtering*, Vol. 5 (Springer, 2020).
- [40] J. Fricks, L. Yao, T. C. Elston, and M. G. Forest, Time-domain methods for diffusive transport in soft matter, *SIAM journal on applied mathematics* **69**, 1277 (2009).
- [41] S. Paul, N. Narinder, A. Banerjee, K. R. Nayak, J. Steindl, and C. Bechinger, Bayesian inference of the viscoelastic properties of a jeffrey's fluid using optical tweezers, *Scientific Reports* **11**, 2023 (2021).
- [42] MathWorks, Var model (varm), <https://in.mathworks.com/help/econ/varm.html>.
- [43] R. Parthasarathy, Rapid, accurate particle tracking by calculation of radial symmetry centers, *Nature Methods*

- [9, 724 \(2012\)](#).
- [44] S. Gupta, A. Khan, P. Biswas, K. Mondal, D. Das, S. Sharif, and A. I. Mallick, A combined protocol for isolation of t6ss-positive campylobacter jejuni and assessment of interspecies interaction, [STAR protocols](#) **3**, 101368 (2022).
- [45] H. Seyforth, M. Gomez, W. B. Rogers, J. L. Ross, and W. W. Ahmed, Nonequilibrium fluctuations and nonlinear response of an active bath, [Physical Review Research](#) **4**, 023043 (2022).